Measurement 254 (2025) 117903

Contents lists available at ScienceDirect

Measurement

journal homepage: www.elsevier.com/locate/measurement

Vector mapping of receiver coordinates to GNSS time transfer

Baoying Wei [a], Kun Liang [a,*], Jian Wang [a], Zhiyu He [b], Yufeng Li [a], Junliang Zhao [a]

[a] School of Automation and Intelligence, Beijing Jiaotong University, Beijing 100044, China
[b] China Academy of Railway Sciences Corporation Limited, Beijing 100081, China

ARTICLE INFO

Keywords:
Time transfer error
Position error
Quantification
Linear relationship
Cosine relationship
Error angle

ABSTRACT

The coordinates of a time transfer station are crucial parameters for time transfer based on Global Navigation Satellite System (GNSS) codes. In dynamic scenarios, larger position errors are introduced, necessitating an analysis and evaluation for the impact of the receiver position error on GNSS time transfer. In this paper, the method for mapping the coordinate vectors of both the receiver and the satellite to GNSS time transfer is proposed. The time transfer error caused by the receiver position error is quantified. The error angle, which can describe the position error of the receiver in three-dimensional space, is defined to characterize the time transfer error along with the position error. An analytical expression describing the relationship between these factors is derived and validated. When the error angle is constant, the time transfer error is approximately linear to the position error. With constant position error, the time transfer error is affected approximately by the cosine function of the error angle.

1. Introduction

In dynamic scenarios, there are increasing requirements for high-precision time synchronization. For instance, the implementation of Multiple-Input Multiple-Output techniques in 5th Generation Mobile Communication Technology for Railways (5G-R) [1] requires that the time difference among system components be less than 65 ns. High-precision time transfer based on Global Navigation Satellite System (GNSS) codes has been extensively developed and widely applied among stationary stations, such as the laboratories contributing to the International Atomic Time (TAI) (see details in [2–4]). As the important known parameters, the coordinates of a time transfer station could be accurately calculated beforehand in stationary stations. In mobile stations, it is difficult to fix the position precisely during a short period so the position errors are larger. Therefore, for GNSS time transfer in mobile stations, it is essential to analyze and evaluate the impact of the station position on time transfer.

Various transmission errors may be introduced into GNSS positioning and timing performance during the propagation of GNSS signals, for instance, the tropospheric effects and the ionospheric effects. The tropospheric delay can be represented with the product of the tropospheric refraction in the zenith direction and a mapping function related to the elevation angle [5]. Traditional models for zenith tropospheric effect correction include the Saastamoinen model in [6] and the Hopfield model in [7]. Mapping functions such as the Niell Mapping Function in [8], the Vienna Mapping Function 1 in [9], and the Global Mapping Function in [10] are widely used. Reference [11] demonstrated that reducing the sampling rate of troposphere parameters to 15 min and applying constraints in Precise Point Positioning (PPP) time transfer could significantly improve clock solution accuracy, reducing errors by up to a factor of 10 for some stations compared to traditional methods. For the single-frequency users, the ionospheric delay can be corrected by the ionospheric models; for the multi-frequency users, ionospheric effects can be eliminated by forming the linear combination of observations. In Global Positioning System (GPS) single-frequency ionospheric delay correction, the impact of the latitudes and the solar activities on the initial phase and nighttime term of the Klobuchar model were studied in [12]. A ten-parameter Klobuchar-like model was proposed, which could improve ionospheric delay correction by 10 % compared to the Klobuchar model. The ionosphere scintillation behavior was studied and modeled in [13]. The effect of the Total Electron Content (TEC) and the Rate of TEC Index on positioning error during solar flares and geomagnetic storms was evaluated in [14]. Reference [15] quantified ionospheric effects on time and frequency transfer solutions. The research showed that the first-order ionospheric delays could reach up to 100 ns (ns) during ionospheric storms, while the second-order delays were about 8 picoseconds (ps) on quiet days and up to 15 ps during ionospheric storms. These delays could significantly impact the accuracy

* Corresponding author.
E-mail address: liangk@bjtu.edu.cn (K. Liang).

https://doi.org/10.1016/j.measurement.2025.117903
Received 27 December 2024; Received in revised form 27 February 2025; Accepted 18 May 2025
Available online 20 May 2025

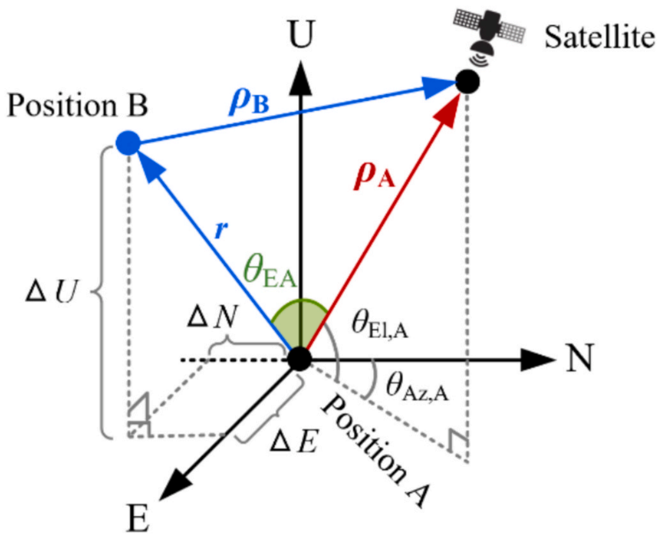

Fig. 1. A local Cartesian coordinate system (E, N, U) with position A as the origin.

of time transfer, especially for long-baseline measurements or during periods of high ionospheric activity. The hardware delays in the satellite and the receiver are also among the errors, with the former obtained from the navigation messages and the latter measured and corrected by calibration techniques. A method called Time Differenced Double Difference Carrier Phase (TDDDCP) to estimate differential phase bias or carrier phase bias of NavIC receiver was proposed by [16]. The carrier phase measurements corrected by the TDDDCP method provided better positioning solutions in the Z-coordinate than those from the DDCP method. Precise time transfer can only be achieved with a calibrated receiver. Hardware delay of an uncalibrated receiver will be introduced into the time transfer results, up to a few hundred nanoseconds. The calibration techniques of the receiver are mainly divided into differential calibration [17] with an uncertainty about 3.4 ns and absolute calibration [18–22] with a total uncertainty better than 2 ns. This means that an uncertainty of several nanoseconds will be introduced into the time transfer results.

In [23], the receiver coordinates with errors were mapped by the satellite coordinates to validate the common sense that a 3-meter position error results in a time transfer error of more than 10 ns. However, the analysis relied solely on the geometric distance between the satellite and the receiver, without considering other factors, such as the ionospheric and tropospheric effects. The proposed time transfer error model only considered the geometric distance and did not explain why ionospheric and tropospheric effects are not included. Reference [24] mentioned the phenomenon where the position error led to significant geometric distance error but caused minor errors in the ionospheric delay and the Sagnac effect. Therefore, the conclusion that the position error had little impact on two-way time transfer is inferred in [24]. However, this inference was based on a phenomenon that lacked quantitative description and theoretical analysis and the time transfer error model had not been proposed. The position of the receiver and the satellite in three-dimensional space can be represented by the coordinate vectors, facilitating precise characterization and analysis. To comprehensively analyze the impact, the position error, which can be represented by coordinate vectors of both the receiver and the satellite, should be mapped into GNSS time transfer. This method is defined as the coordinate vector mapping in this paper and is used to study the impact of the position error on time transfer. The coordinate vectors of both the receiver and the satellite will be defined. The effects of the correction terms of the transmission errors in time transfer will be analyzed individually. The combined impact of these effects on time transfer will be studied. After the theoretical analysis, an analytical expression of time transfer error caused by the position error will be proposed in this paper.

2. Coordinate vectors and GNSS observation

A Cartesian coordinate system is defined in this section for describing the coordinate vectors of the receiver and the satellite. Since GNSS time transfer is conducted based on GNSS observation equations, this section will present the expressions for the observation equations based on the coordinate vectors.

2.1. Coordinate vectors of the receiver and the satellite

Position A and position B are defined to represent the true position and the position with an error. A local Cartesian coordinate system (E, N, U) with position A as the origin is constructed as shown in Fig. 1, whose E-axis points to the east and N-axis points to the north. $\boldsymbol{\rho}_{\mathrm{A}}$ and $\boldsymbol{\rho}_{\mathrm{B}}$ are the vector from position A to the satellite and the vector from position B to the satellite, respectively. $\boldsymbol{r}$ is the vector from position A to position B. The module of $\boldsymbol{r}$ is defined as the position error. ΔE, ΔN and ΔU are the projection of $\boldsymbol{r}$ onto the E-axis, the N-axis and the U-axis, respectively, which are defined as the coordinate errors. The relationship between the position error and the coordinate errors is expressed as follows:

$$\|\boldsymbol{r}\| = \sqrt{\Delta E^2 + \Delta N^2 + \Delta U^2} \tag{1}$$

$\theta_{\mathrm{El,A}}$ and $\theta_{\mathrm{Az,A}}$ are the elevation and the azimuth of the satellite observed at position A. The angle between $\boldsymbol{\rho}_{\mathrm{A}}$ and $\boldsymbol{r}$ is defined as the error angle θ_{EA}.

2.2. Relationship between time transfer error and GNSS observation

The pseudorange measurement on single-frequency is used to comprehensively analyze the correction terms of errors in GNSS time transfer including the ionospheric effects. $T_{\mathrm{L\text{-}G}}$ is the time difference between the local clock and the GNSS system time (GNSS-T) and can be calculated as (2) and (3), with the principles detailed in [25]. The subscript A/B indicates that this is a variable based on position A/B.

$$T_{\mathrm{L\text{-}G,A}} = \frac{1}{c}\left(P_{\mathrm{A}} - \|\boldsymbol{\rho}_{\mathrm{A}}\| - S_{\mathrm{A}}\right) + T_{\mathrm{rel,A}} - T_{\mathrm{tropo,A}} - T_{\mathrm{iono,A}} - GD_{\mathrm{A}} + T_{\mathrm{sat,A}} \tag{2}$$

$$T_{\mathrm{L\text{-}G,B}} = \frac{1}{c}\left(P_{\mathrm{B}} - \|\boldsymbol{\rho}_{\mathrm{B}}\| - S_{\mathrm{B}}\right) + T_{\mathrm{rel,B}} - T_{\mathrm{tropo,B}} - T_{\mathrm{iono,B}} - GD_{\mathrm{B}} + T_{\mathrm{sat,B}} \tag{3}$$

c is the velocity of the light. P is the pseudorange measurement, which has been corrected with the hardware delays of the GNSS time transfer receiver. $\|\boldsymbol{\rho}_{\mathrm{A}}\|$ and $\|\boldsymbol{\rho}_{\mathrm{B}}\|$ are the geometric distances from positions A and B to the satellite separately. S is the Sagnac correction associated with the earth's rotation. T_{rel} is the relativistic clock correction. T_{iono} and T_{tropo} are the ionospheric delay and the tropospheric delay, respectively. GD is the broadcast group delay. T_{sat} is the satellite clock correction. S, T_{rel}, GD and T_{sat}, which can be calculated by the known parameters and the correction models, such as the rotational speed of the earth, are independent of the receiver coordinates. If the pseudorange measurement P_{A} and P_{B} at positions A and B are constrained to be equal, the time transfer error $\Delta T_{\mathrm{L\text{-}G}}$ caused by the position error can be expressed as follows:

$$\begin{aligned} \Delta T_{\mathrm{L\text{-}G}} &= T_{\mathrm{L\text{-}G,B}} - T_{\mathrm{L\text{-}G,A}} \\ &= \frac{1}{c}\left(\|\boldsymbol{\rho}_{\mathrm{A}}\| - \|\boldsymbol{\rho}_{\mathrm{B}}\|\right) + T_{\mathrm{tropo,A}} - T_{\mathrm{tropo,B}} + T_{\mathrm{iono,A}} - T_{\mathrm{iono,B}} \end{aligned} \tag{4}$$

3. Coordinate vectors mapping to GNSS time transfer

From (4) in section 2.2, it can be seen that the time transfer error is affected by the geometric distance, the ionospheric delay, and the tropospheric delay. The impact of the position error on the three types of delay will be analyzed in sections 3.1 to 3.3. In section 3.4, the combined

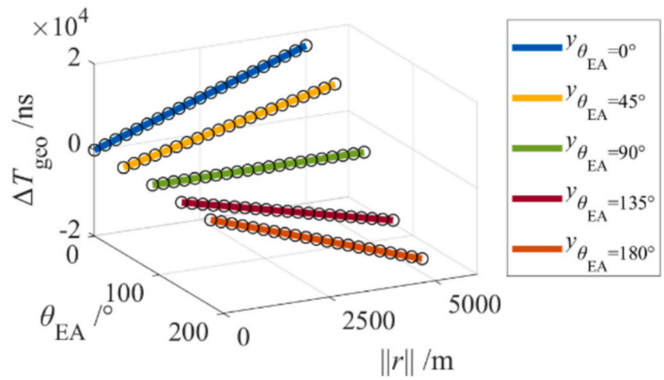

Fig. 2. The values of ΔT_{geo} correspond to different values of $\|\boldsymbol{r}\|$ and θ_{EA}. The functions used for fitting are: $y_{\theta_{\mathrm{EA}}=0^\circ} = 3.34\|\boldsymbol{r}\|$, $y_{\theta_{\mathrm{EA}}=45^\circ} = 2.36\|\boldsymbol{r}\|$, $y_{\theta_{\mathrm{EA}}=90^\circ} = 0\|\boldsymbol{r}\|$, $y_{\theta_{\mathrm{EA}}=135^\circ} = -2.36\|\boldsymbol{r}\|$, $y_{\theta_{\mathrm{EA}}=180^\circ} = -3.34\|\boldsymbol{r}\|$.

impact on GNSS time transfer will be studied.

3.1. Geometric distance delay

The signal propagation delay caused by the geometric distance between the satellite and the receiver is defined as the geometric distance delay. The impact of the position error on the geometric distance delay will be analyzed through theoretical analysis and data fitting. ΔT_{geo} is the error of the geometric distance delay caused by the position error, and it can be calculated as follows:

$$\Delta T_{\mathrm{geo}} = \frac{\|\boldsymbol{\rho}_{\mathrm{A}}\| - \|\boldsymbol{\rho}_{\mathrm{B}}\|}{c} = \frac{\|\boldsymbol{\rho}_{\mathrm{A}}\| - \sqrt{\|\boldsymbol{r}\|^2 + \|\boldsymbol{\rho}_{\mathrm{A}}\|^2 - 2\|\boldsymbol{r}\|\|\boldsymbol{\rho}_{\mathrm{A}}\|\cos\theta_{\mathrm{EA}}}}{c} \tag{5}$$

$\|\boldsymbol{r}\|$ and θ_{EA} are both independent variables of ΔT_{geo}. Eqs. (6) and (7) are the first and the second order derivative functions of ΔT_{geo} with respect to $\|\boldsymbol{r}\|$, respectively.

$$[\Delta T_{\mathrm{geo}}]'_{\|\boldsymbol{r}\|} = -\frac{\|\boldsymbol{r}\| - \|\boldsymbol{\rho}_{\mathrm{A}}\|\cos\theta_{\mathrm{EA}}}{c\sqrt{\|\boldsymbol{r}\|^2 + \|\boldsymbol{\rho}_{\mathrm{A}}\|^2 - 2\|\boldsymbol{r}\|\|\boldsymbol{\rho}_{\mathrm{A}}\|\cos\theta_{\mathrm{EA}}}} \tag{6}$$

$$[\Delta T_{\mathrm{geo}}]''_{\|\boldsymbol{r}\|} = \frac{\|\boldsymbol{\rho}_{\mathrm{A}}\|^2(\cos^2\theta_{\mathrm{EA}} - 1)}{c\left(\|\boldsymbol{r}\|^2 + \|\boldsymbol{\rho}_{\mathrm{A}}\|^2 - 2\|\boldsymbol{r}\|\|\boldsymbol{\rho}_{\mathrm{A}}\|\cos\theta_{\mathrm{EA}}\right)^{1.5}} \tag{7}$$

To make the analysis more realistic, the maximum position error of 5000 meters (m), which is the worst case of the international search and rescue services [26] for the Beidou Navigation Satellite System (BDS), is taken as an example. The maximum value of $\|\boldsymbol{r}\|$ is set to 5000 m. θ_{EA} varies from 0° to 180°. In light of the fact that $\|\boldsymbol{r}\|$ is much smaller than $\|\boldsymbol{\rho}_{\mathrm{A}}\|$ by tens of thousands of kilometers (km), the value of $[\Delta T_{\mathrm{geo}}]''_{\|\boldsymbol{r}\|}$ can be estimated. When θ_{EA} is 0° or 180°, $[\Delta T_{\mathrm{geo}}]''_{\|\boldsymbol{r}\|}$ reaches the maximum value of 0; when θ_{EA} is 90°, $[\Delta T_{\mathrm{geo}}]''_{\|\boldsymbol{r}\|}$ reaches the minimum value of $-\|\boldsymbol{\rho}_{\mathrm{A}}\|^2/[c(\|\boldsymbol{r}\|^2 + \|\boldsymbol{\rho}_{\mathrm{A}}\|^2)^{1.5}]$, which approximates to 0. It can be deduced that $[\Delta T_{\mathrm{geo}}]'_{\|\boldsymbol{r}\|}$ can be regarded as a constant. Therefore, an approximately linear relationship between $\|\boldsymbol{r}\|$ and ΔT_{geo} can be inferred and expressed as (8). k is the proportional factor and depends only on θ_{EA} and $\|\boldsymbol{r}\|$. When θ_{EA} is 0°, k reaches its maximum value of $1/c$; when θ_{EA} is 90° or 180°, k reaches its minimum value of $-1/c$.

$$\begin{cases} \Delta T_{\mathrm{geo}} = k\|\boldsymbol{r}\| \\ k = [\Delta T_{\mathrm{geo}}]'_{\|\boldsymbol{r}\|} = -\dfrac{\|\boldsymbol{r}\| - \|\boldsymbol{\rho}_{\mathrm{A}}\|\cos\theta_{\mathrm{EA}}}{c\sqrt{\|\boldsymbol{r}\|^2 + \|\boldsymbol{\rho}_{\mathrm{A}}\|^2 - 2\|\boldsymbol{r}\|\|\boldsymbol{\rho}_{\mathrm{A}}\|\cos\theta_{\mathrm{EA}}}} \end{cases} \tag{8}$$

A satellite with a lower orbital altitude exhibits a larger difference

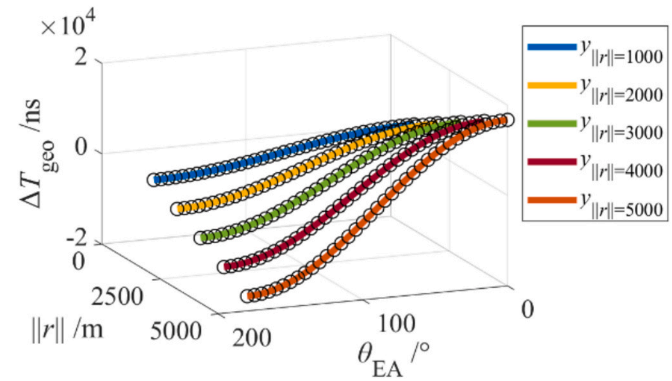

Fig. 3. The values of ΔT_{geo} correspond to different values of $\|\boldsymbol{r}\|$ and θ_{EA}. The functions used for fitting are: $y_{\|\boldsymbol{r}\|=1000} = 3340\cos(\theta_{\mathrm{EA}})$, $y_{\|\boldsymbol{r}\|=2000} = 6670\cos(\theta_{\mathrm{EA}})$, $y_{\|\boldsymbol{r}\|=3000} = 10000\cos(\theta_{\mathrm{EA}})$, $y_{\|\boldsymbol{r}\|=4000} = 13300\cos(\theta_{\mathrm{EA}})$, $y_{\|\boldsymbol{r}\|=5000} = 16700\cos(\theta_{\mathrm{EA}})$.

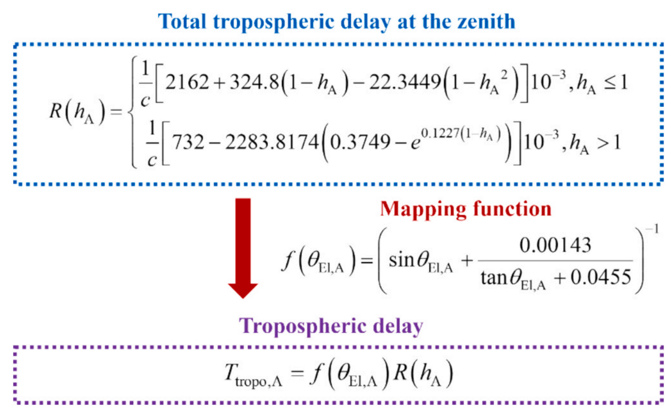

Fig. 4. The calculation process of the tropospheric delay $T_{\mathrm{tropo,A}}$ at position A.

between $\|\boldsymbol{\rho}_{\mathrm{A}}\|$ and $\|\boldsymbol{\rho}_{\mathrm{B}}\|$ for the same $\|\boldsymbol{r}\|$, which results in a larger ΔT_{geo}. Therefore, the BDS Medium Earth Orbit (MEO) satellite with an orbital altitude of 21528 km is selected for ΔT_{geo} calculation. Based on the geometric relationship shown in Fig. 1, the corresponding values of ΔT_{geo} to different values of $\|\boldsymbol{r}\|$ and θ_{EA} can be calculated, which are the black hollow dots shown in Fig. 2. The linear function $y_{\theta_{\mathrm{EA}}}$ is used to fit the values of ΔT_{geo} when θ_{EA} are 0°, 45°, 90°, 135°, and 180°, respectively. By adjusting the proportional factor of the linear function, the fitting of ΔT_{geo} can be achieved. The conclusion inferred from the good fit phenomenon is that when θ_{EA} is constant, the relationship between $\|\boldsymbol{r}\|$ and ΔT_{geo} can be approximated as a linear relationship.

θ_{EA} influences ΔT_{geo}, in conjunction with $\|\boldsymbol{r}\|$. Thus, it is necessary to analyze the relationship between ΔT_{geo} and θ_{EA}. The relationship between them can be approximated by data fitting. In Fig. 3, in the cases of different constant values of $\|\boldsymbol{r}\|$, the values of ΔT_{geo} can be fitted by different cosine functions with different values of amplitude. Therefore, when $\|\boldsymbol{r}\|$ is held constant, the relationship between ΔT_{geo} and θ_{EA} can be approximated by a cosine function, as expressed in (9). A is the amplitude of the cosine function.

$$\Delta T_{\mathrm{geo}} = A\cos\theta_{\mathrm{EA}} \tag{9}$$

In the case where $\|\boldsymbol{r}\|$ is 5000 m and $\|\boldsymbol{\rho}_{\mathrm{A}}\|$ is 21528 km, the maximum of ΔT_{geo} is 16678.2 ns and the minimum is 1.9 ns. For the more common case where $\|\boldsymbol{r}\|$ is 5 m, the maximum and minimum values of ΔT_{geo} are 16.7 ns and 1.5×10^{-6} ns, respectively.

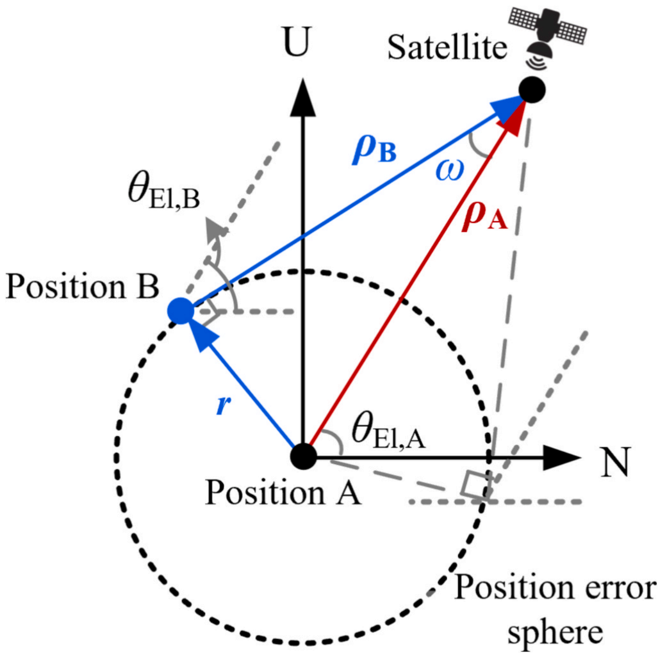

Fig. 5. Diagram of the position error sphere.

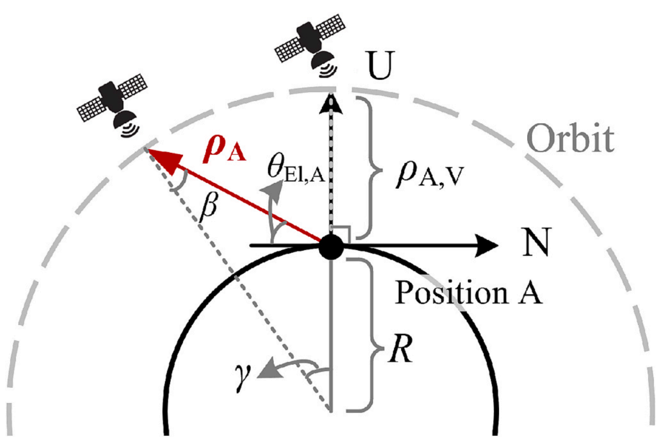

Fig. 6. Different values of elevation $\theta_{El,A}$ result in different values of $\|\boldsymbol{\rho}_A\|$.

3.2. Tropospheric delay

The tropospheric delay $T_{tropo,A}$ at position A, computed by the standard North Atlantic Treaty Organization (NATO) hydrostatic model, is calculated following the procedure shown in Fig. 4. $f(\theta_{El,A})$ is a tropospheric mapping function of the elevation $\theta_{El,A}$. $\Delta R(h_A)$ is the total tropospheric delay at the zenith for the ellipsoidal height h_A of position A.

$\theta_{El,B}$ and h_B are the elevation of the satellite observed at position B and the ellipsoidal height of position B, respectively. The NATO hydrostatic model is used for the computation of the tropospheric delay $T_{tropo,B}$ at position B. $f(\theta_{El,B})$ is the tropospheric mapping function of $\theta_{El,B}$. $\Delta R(h_B)$ is the total tropospheric delay at the zenith for h_B. The tropospheric delay error ΔT_{tropo} caused by the position error can be calculated as follows:

$$\begin{aligned}\Delta T_{tropo} &= T_{tropo,B} - T_{tropo,A}\\ &= f(\theta_{El,B})R(h_B) - f(\theta_{El,A})R(h_A)\end{aligned} \tag{10}$$

The impact of the position error $\|\boldsymbol{r}\|$ on the tropospheric mapping function is analyzed first. The position error sphere with radius $\|\boldsymbol{r}\|$, is shown in Fig. 5. The angle between $\boldsymbol{\rho}_A$ and $\boldsymbol{\rho}_B$ is defined as ω. When the line defined by $\boldsymbol{\rho}_B$ is tangent to the position error sphere, ω reaches the maximum value, denoted as ω_{max}, which is expressed as

$$\omega_{max} = \arcsin\left(\frac{\|\boldsymbol{r}\|}{\|\boldsymbol{\rho}_A\|}\right) \tag{11}$$

In order to estimate the range of $\theta_{El,B}$, only the maximum value ω_{max} of ω is considered. As shown in Fig. 6, different values of $\theta_{El,A}$ result in different values of $\|\boldsymbol{\rho}_A\|$. The earth is considered as a sphere with the earth's mean spherical radius R. $\rho_{A,V}$ is the geometric distance between the satellite and position A when the satellite over position A. γ is an angle defined for auxiliary calculation. $\|\boldsymbol{\rho}_A\|$ can be treated as a dependent variable of $\theta_{El,A}$ and expressed as follows:

$$\|\boldsymbol{\rho}_A\| = \frac{(\rho_{A,V} + R)\sin\gamma}{\sin(\theta_{El,A} + 90^\circ)} \tag{12}$$

$$\gamma = 90^\circ - \theta_{El,A} - \beta \tag{13}$$

$$\beta = \arcsin\left(\frac{R\sin(\theta_{El,A} + 90^\circ)}{(\rho_{A,V} + R)}\right) \tag{14}$$

$\|\boldsymbol{r}\|$ is set to 5000 m. In order to maximize ω_{max}, $\rho_{A,V}$ is set to 21528 km, which is the altitude of the BDS MEO satellite. The corresponding values of ω_{max} to different values of $\theta_{El,A}$ are shown in Fig. 7. Since $\sin(\theta_{El,A} + 90^\circ)$, which is the denominator of (12), cannot be 0, the value of ω_{max} when $\theta_{El,A}$ of 90° is not calculated. The phenomenon that the higher $\theta_{El,A}$ leads to the larger ω_{max} is demonstrated in Fig. 7. With a difference of no more than 0.003° between the maximum and minimum values of ω_{max}, ω_{max} takes the maximum value of 0.0133° in the subsequent analysis, regardless of the different values of $\theta_{El,A}$. Therefore, when the position error is 5000 m, $\theta_{El,B}$ is within the interval $[\theta_{El,A} - 0.0133^\circ, \theta_{El,A} + 0.0133]$. Fig. 8 shows $f(\theta_{El,A})$ for varying $\theta_{El,A}$. As $\theta_{El,A}$ increases, both the rate of change and the value of $f(\theta_{El,A})$ decrease. This relationship also holds between $\theta_{El,B}$ and $f(\theta_{El,B})$. As the midpoint of the interval for $\theta_{El,B}$, a lower $\theta_{El,A}$ results in a larger difference between $f(\theta_{El,A})$ and $f(\theta_{El,B})$, which may lead to a larger ΔT_{tropo} according to (10). Since $(\theta_{El,A} - 0.0133^\circ)$ becomes negative when $\theta_{El,A}$ is smaller than 0.0133°, $\theta_{El,A}$ is taken as 0.0133°.

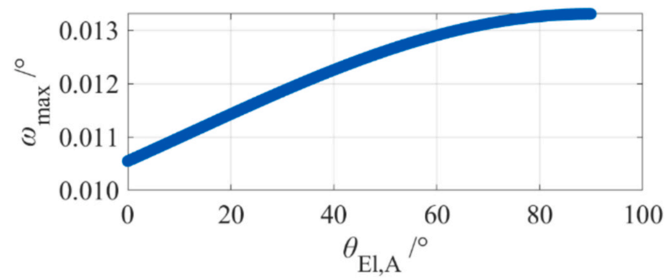

Fig. 7. The values of ω_{max} correspond to different values of $\theta_{El,A}$.

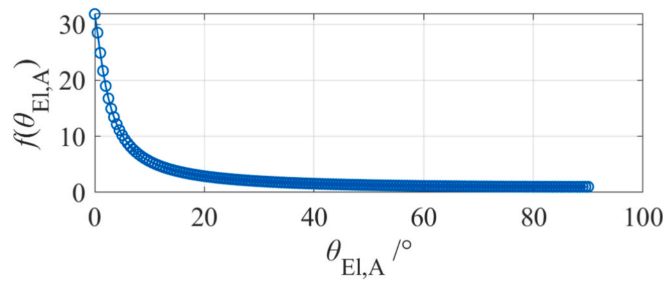

Fig. 8. The values of $f(\theta_{El,A})$ correspond to different values of $\theta_{El,A}$.

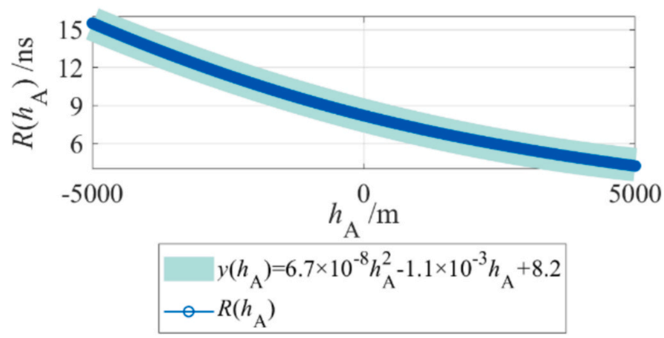

Fig. 9. The values of $\Delta R(h_A)$ correspond to different values of h_A.

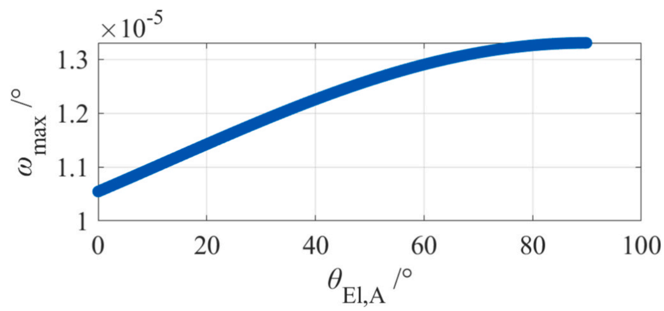

Fig. 10. The values of ω_{max} correspond to different values of $\theta_{El,A}$ when $\|\boldsymbol{r}\|$ is 5 m.

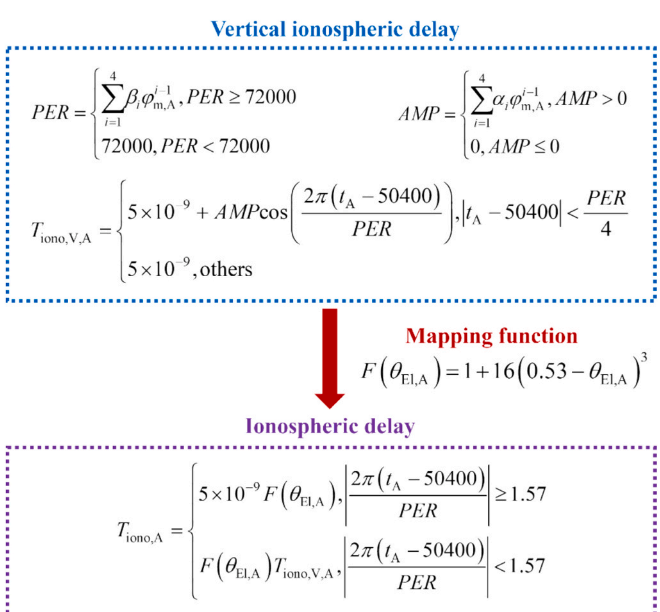

Fig. 11. The calculation process of the ionospheric delay $T_{iono,A}$ at position A.

The impact of the position error on the total tropospheric delay at the zenith is analyzed secondly. The values of $R(h_A)$ corresponding to h_A from -5000 m to 5000 m are shown in Fig. 9. The portion of the parabola $y(h_T)$ to the left of the vertex can be used to fit $R(h_A)$, which means that both the rate of change and the value of $R(h_A)$ decrease as h_A increases. A smaller h_A, combined with a larger difference between h_A and h_B, will result in a larger ΔT_{tropo}. Since the earth is modeled as a sphere, the difference between h_A and h_B is considered as the projection of $\boldsymbol{r}$ on the U-axis. It can be inferred that ΔU should be as large as possible to obtain a larger ΔT_{tropo}.

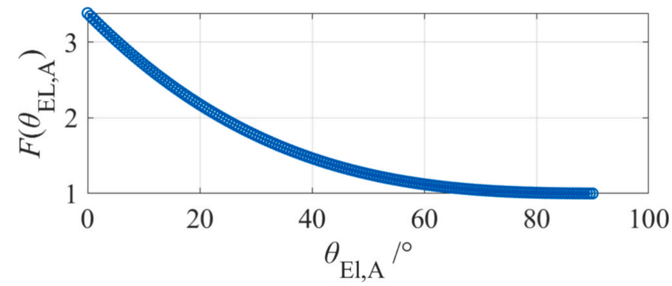

Fig. 12. The values of $F(\theta_{El,A})$ correspond to different values of $\theta_{El,A}$.

A special case is set to find the maximum of ΔT_{tropo}, where h_A is 0 m, $\theta_{El,A}$ is 0°, $\|\boldsymbol{r}\|$ is 5000 m, h_E is -5000 m. In this case, even though the actual value of ω_{max} is less than 0.0133°, it is set to 0.0133° to maximize the difference between $f(\theta_{El,A})$ and $f(\theta_{El,B})$. Then ΔT_{tropo} is calculated to be 230.6 ns. That is, a position error of 5000 m will result in a maximum tropospheric delay error of 230.6 ns. In the case where $\|\boldsymbol{r}\|$ is 5 m, the corresponding values of ω_{max} to different values of $\theta_{El,A}$ are shown in Fig. 10. When h_B and h_A are -5000 m and -4995 m, respectively, the maximum tropospheric delay error is 0.3 ns.

3.3. Ionospheric delay

The calculation process of ionospheric delay $T_{iono,A}$ at position A based on the Klobuchar model is shown in Fig. 11. The vertical ionospheric delay $T_{iono,V,A}$ is fitted by a positive half cosine function of t_A, which is the local time at the Ionospheric Pierce Point (IPP). *AMP* and *PER* are the amplitude and the period of the positive half cosine function. $\varphi_{m,A}$ is the geomagnetic latitude of IPP, which can be calculated by the latitude, the longitude, $\theta_{Az,A}$ and $\theta_{El,A}$. α_i and β_i are the ionospheric parameters obtained from the GNSS navigation message. The ionospheric delay $T_{iono,A}$ at position A can be converted from $T_{iono,V,A}$ with an ionospheric mapping function $F(\theta_{El,A})$.

The ionospheric delay error ΔT_{iono} caused by the position error can be expressed as follows:

$$\Delta T_{iono}=T_{iono,B}-T_{iono,A}$$
$$=\begin{cases}5\times10^{-9}\left(F(\theta_{El,B})-F(\theta_{El,A})\right), \left|\dfrac{2\pi(t_{A/B}-50400)}{PER}\right|\geq1.57\\ F(\theta_{El,B})T_{iono,V,B}-F(\theta_{El,A})T_{iono,V,A}, \left|\dfrac{2\pi(t_{A/B}-50400)}{PER}\right|<1.57\end{cases} \tag{15}$$

$T_{iono,B}$ is the ionospheric delay at position B calculated by the Klobuchar model. $T_{iono,V,B}$ and $\theta_{El,B}$ are the vertical ionospheric delay and the elevation of position B, respectively. The subscript A/B indicates that both t_A and t_B satisfy the same condition. In the case of $|2\pi(t_{A/B}-50400)/PER|\geq1.57$, that is, during the nighttime, ΔT_{iono} depends only on $\theta_{El,A}$ and $\theta_{El,B}$. Fig. 12 shows the values of $F(\theta_{El,A})$ correspond to different values of $\theta_{El,A}$. As $\theta_{El,A}$ increases, both the rate of change and the value of $f(\theta_{El,A})$ decrease. ω_{max} caused by the position error $\|\boldsymbol{r}\|$ has been calculated in section 3.2. Therefore, the maximum absolute value of ΔT_{iono} during the nighttime can be calculated based on $F(\theta_{El,T}=0^\circ)$ and $F(\theta_{El,E}=\omega_{max})$, which are 5.0×10^{-3} ns when $\|\boldsymbol{r}\|$ is 5000 m and 5.0×10^{-6} ns when $\|\boldsymbol{r}\|$ is 5 m.

In the case of $|2\pi(t_{A/B}-50400)/PER|<1.57$, $T_{iono,V,A}$ is determined by the geographic longitude, the latitude, $\theta_{Az,A}$, $\theta_{El,A}$ and t_A. Since there are too many parameters that need to be analyzed, $T_{iono,V,A}$ will be calculated by traversing parameters to find those that lead to the fastest rate of change in the vertical ionospheric delay. t_A is determined by the GNSS signal transmission time and the position of IPP. Since $T_{iono,V,A}$ is

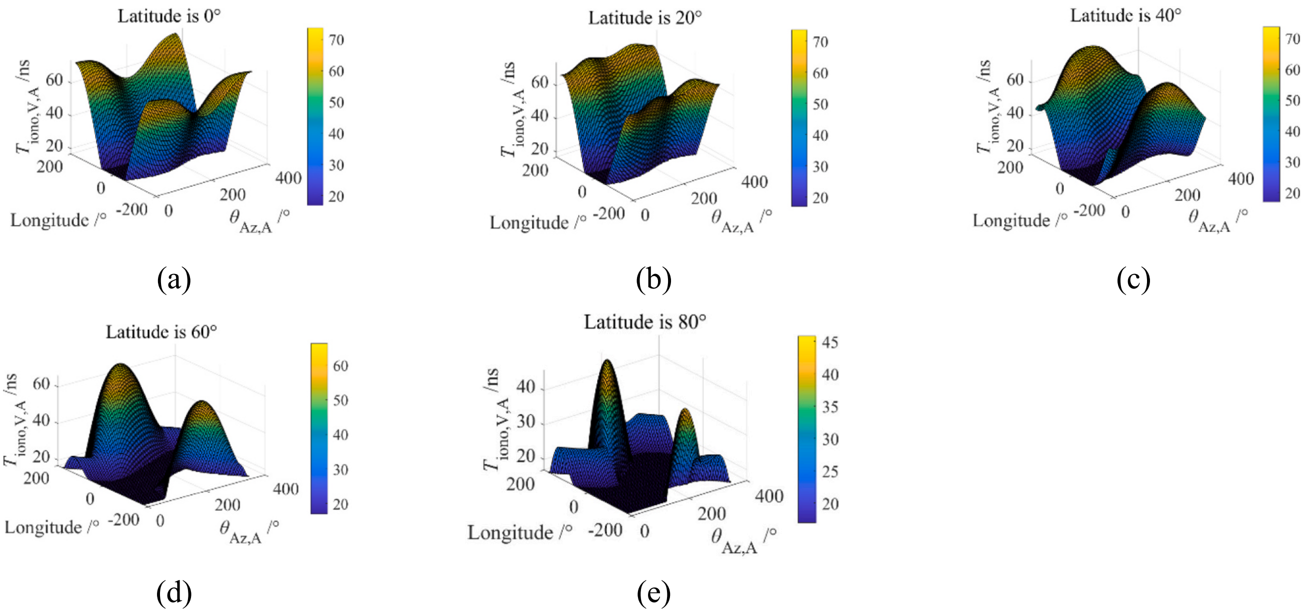

Fig. 13. The values of $T_{\mathrm{iono,V,A}}$ correspond to different values of the latitude, the longitude, and $\theta_{\mathrm{Az,A}}$.

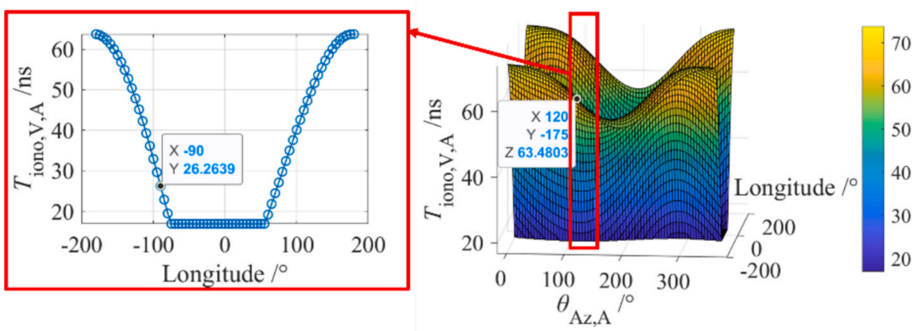

Fig. 14. The values of $T_{\mathrm{iono,V,T}}$ correspond to different values of $\theta_{\mathrm{Az,A}}$ and the longitude when latitude is 0°.

calculated by traversing the parameters including t_{A}, the GNSS signal transmission time can be taken as any epoch within a GPS week. $\theta_{\mathrm{El,A}}$ is taken as 0° to ensure that $F(\theta_{\mathrm{El,A}})$ achieves both its maximum value and rate of change, providing $T_{\mathrm{iono,A}}$ with the opportunity to reach its maximum. The ionospheric parameters are derived from the broadcast ephemeris on September 5, 2023. The corresponding values of $T_{\mathrm{iono,V,A}}$ to different values of latitude (only the northern hemisphere is considered), longitude, and $\theta_{\mathrm{Az,A}}$ are shown from Fig. 13(a)–(e).

Fig. 13(a) to Fig. 14(e) illustrate that $T_{\mathrm{iono,V,A}}$ decreases as the latitude of position A increases, suggesting that the maximum value of $T_{\mathrm{iono,V,A}}$ may occur in low-latitude areas. Therefore, the latitude of position A is set to 0°. The rate of change of $T_{\mathrm{iono,V,A}}$ with respect to $\theta_{\mathrm{Az,A}}$ is shown in Fig. 14. The corresponding values of $\theta_{\mathrm{Az,A}}$ and longitude when $T_{\mathrm{iono,V,A}}$ reaches its maximum rate of change can be estimated as 120° and −90°, respectively.

When $\|\boldsymbol{r}\|$ of 5000 m is on the E-N plane, the values of longitude and the latitude of position B are within the ranges [-89.9551°, −90.0449°] and [-0.0452°, 0.0452°], respectively. In this case, the change of the latitude and the longitude are too small to traverse them to cover the position of the IPP. Therefore, the selection of t_{A} needs to be considered. Since the positive half cosine function is used to fit the vertical ionospheric delay except the nighttime period, the closer t_{A} approaches the endpoints of the nighttime interval, the greater the rate of change of the vertical ionospheric delay. The position error will make t_{A} change to t_{B}, which is the local time at IPP of position B. Therefore, t_{A} is selected close

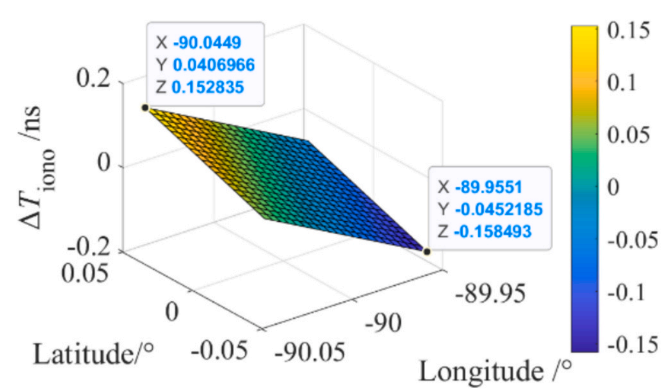

Fig. 15. The corresponding values of ΔT_{iono} to different longitude and latitude values of position B when the position error is 5000 m.

to the values of the endpoints (6 h and 22 h) but not exactly at them, to prevent $T_{\mathrm{iono,V,A}}$ from becoming a constant when t_{B} is within the nighttime period. t_{A} is obtained by converting an observation epoch on September 5, 2023, which is about 21 h at position A.

When the position error is 5000 m, the corresponding values of ΔT_{iono} to different values of longitude and latitude of position B are shown in Fig. 15. The absolute value of ΔT_{iono}, $|T_{\mathrm{iono}}|$, is used to quantify

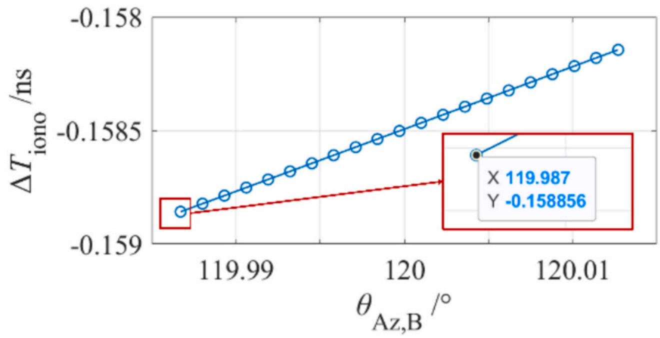

Fig. 16. The values of ΔT_{iono} correspond to different azimuth values of position B.

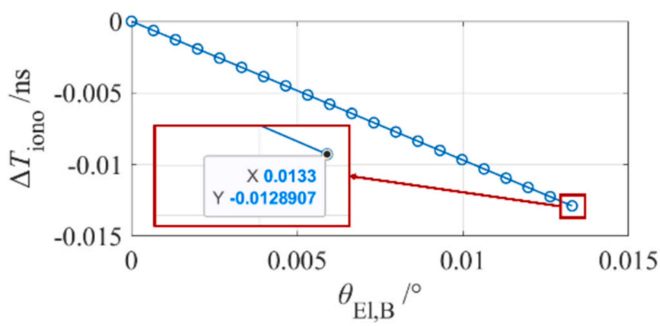

Fig. 17. The values of ΔT_{iono} correspond to different values of $\theta_{\mathrm{El,B}}$.

the impact of the position error on ionospheric delay. The maximum $|T_{\mathrm{iono}}|$ is 1.6×10^{-1} ns, which corresponds to position B with geographic coordinates (0.0452°S, 89.9551°W). If $\|\boldsymbol{r}\|$ decreases, that is, the difference of longitude and latitude between position B and position A decreases, then $|T_{\mathrm{iono}}|$ must be less than 1.6×10^{-1} ns.

The maximum value of $|T_{\mathrm{iono}}|$ is further analyzed with consideration of the azimuth. The maximum difference between the azimuth $\theta_{\mathrm{Az,B}}$ of position B and $\theta_{\mathrm{Az,A}}$ caused by $\|\boldsymbol{r}\|$ of 5000 m is 0.0266°, of which calculation is shown in section 3.2. In Fig. 16, when $\theta_{\mathrm{Az,B}}$ is 119.9870°, $|T_{\mathrm{iono}}|$ achieves its maximum 1.6×10^{-1} ns. Since $|T_{\mathrm{iono}}|$ analyzed above is based on position B (0.0452°S, 89.9551°W), that is, $\|\boldsymbol{r}\|$ is 7070 m, the maximum value of $|T_{\mathrm{iono}}|$ when $\|\boldsymbol{r}\|$ is 5000 m will be actually smaller than 1.6×10^{-1} ns. In other words, the ionospheric delay error caused by 5000 m position error is no more than 1.6×10^{-1} ns.

When the projection of $\boldsymbol{r}$ on the U-axis is not zero, $\theta_{\mathrm{El,B}}$ is the only variable in the calculation of ΔT_{iono}. $\theta_{\mathrm{El,B}}$ varies from 0° to 0.0133°, and the corresponding values of ΔT_{iono} are shown in Fig. 17. The maximum $|T_{\mathrm{iono}}|$ is 1.3×10^{-2} ns when $\theta_{\mathrm{El,B}}$ is 0.0133°. The maximum ionospheric delay error is estimated jointly by the position error occurring in the N-E plane and the U-axis. In this way, the ionospheric delay error caused by 5000 m position error is no more than 1.7×10^{-1} ns, which is the sum of 1.6×10^{-1} ns and 1.3×10^{-2} ns.

The same method is used for the analysis of 5 m position error and the ionospheric delay error is no more than 1.7×10^{-4} ns.

3.4. Combined impact on time transfer

The results from Sections 3.1 to 3.3 indicate that the largest magnitude of the error caused by the position error occurs in the geometric distance delay. Therefore, ΔT_{geo}, $\Delta T_{\mathrm{tropo}}$, and ΔT_{iono} are compared in the scenario where ΔT_{geo} is minimized, while $\Delta T_{\mathrm{tropo}}$ and ΔT_{iono} are maximized. This scenario occurs when $\theta_{\mathrm{El,A}}$ is 0.0133° and both ΔE and ΔN are zero, as discussed in Sections 3.2 and 3.3. When $\|\boldsymbol{r}\|$ is 5000 m, ΔT_{geo} is calculated to be 1533.8 ns by (5), which is 6 times larger than $\Delta T_{\mathrm{tropo}}$ of 230.6 ns and 8927 times larger than ΔT_{iono} of 1.7×10^{-1} ns.

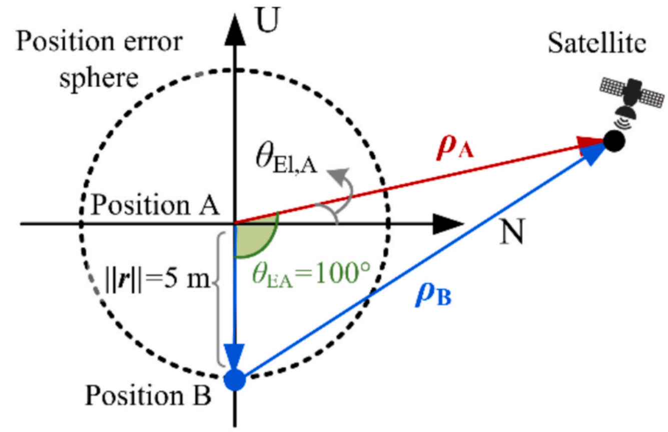

Fig. 18. The scenario where $\theta_{\mathrm{El,A}}$ is 10° and $\|\boldsymbol{r}\|$ is 5 m.

However, when $\|\boldsymbol{r}\|$ is 5 m, ΔT_{geo} of 1.5×10^{-6} ns calculated by (5) is smaller than $\Delta T_{\mathrm{tropo}}$ of 0.3 ns. Since the elevation of 0° is not common and it is the value of elevation mask angle set in R2CGGTTSv8.8 software, which is used for experiments, the analysis was conducted with $\theta_{\mathrm{El,A}}$ of 10°. The scenario where the absolute value of ΔU is equal to $\|\boldsymbol{r}\|$ and θ_{EA} is 100° is shown in Fig. 18, making ΔT_{geo} of 2.9 ns and $\Delta T_{\mathrm{tropo}}$ of 5.1×10^{-2} ns. ΔT_{geo} will increase with the change of θ_{EA} when θ_{EA} is within the interval [0°, 80°] ∪ [100°, 180°]. But $\Delta T_{\mathrm{tropo}}$ will not exceed 5.1×10^{-2} ns. These results show that, when the position error is 5 m, ΔT_{geo} will be two orders of magnitude larger than $\Delta T_{\mathrm{tropo}}$ in about 89 % of the cases ([0°, 80°] ∪ [100°, 180°])/180°≈0.89). The ratio of 89 % will increase as the position error increases.

ΔT_{iono} when $\theta_{\mathrm{El,A}}$ is 10° is no longer calculated since it is less than 1.7×10^{-4} ns, which is its maximum value and four orders of magnitude smaller than ΔT_{geo} of 2.9 ns.

In summary, when θ_{EA} is within the interval [0°, 80°] ∪ [100°, 180°], ΔT_{geo} is two orders of magnitude larger than $\Delta T_{\mathrm{tropo}}$ and four orders of magnitude lager than ΔT_{iono}. Therefore, compared with the geometric distance delay error caused by the position error, the tropospheric delay error and the ionospheric delay error can be ignored. The time transfer error $\Delta T_{\mathrm{L-G}}$ can be estimated to ΔT_{geo} and calculated by (16) and (17). The linear and cosine relationships between $\|\boldsymbol{r}\|$, θ_{EA}, and ΔT_{geo} extend to $\Delta T_{\mathrm{L-G}}$.

$$\begin{cases} \Delta T_{\mathrm{L-G}} = k\|\boldsymbol{r}\| \\ k = -\dfrac{\|\boldsymbol{r}\| - \|\boldsymbol{\rho}_{\mathrm{A}}\|\cos\theta_{\mathrm{EA}}}{c\sqrt{\|\boldsymbol{r}\|^2 + \|\boldsymbol{\rho}_{\mathrm{A}}\|^2 - 2\|\boldsymbol{r}\|\|\boldsymbol{\rho}_{\mathrm{A}}\|\cos\theta_{\mathrm{EA}}}} \end{cases} \tag{16}$$

$$\Delta T_{\mathrm{L-G}} = A\cos\theta_{\mathrm{EA}} \tag{17}$$

4. Experiments and results

In order to validate that the time transfer error is mainly caused by the geometric distance delay error and to evaluate the accuracy of (16) and (17), two experiments are designed. In experiment 1, comparisons will be made between the time transfer error, the tropospheric delay error, the ionospheric delay error, and the geometric distance delay error caused by different position errors. Experiment 2 will compare the theoretical time transfer error calculated based on (16) with the true time transfer error, and try to use the cosine function in the form of (17) to fit the true time transfer error when the position error is constant. The residuals are calculated to evaluate the performance of (16) and the cosine function fitting. Both experiments are based on real GNSS observation data.

Table 1
$\theta_{El,A}$ of BDS and GPS Satellites.

PRN	C05	C02	C28	C41	G32	G04	G16
$\theta_{El,A}/^\circ$	15.9	33.6	53.9	85.2	15.4	35.3	60.2

4.1. Experiments setup

The GNSS time transfer receiver BJ02 referenced to TS(BJTU), which is an atomic time scale kept by our laboratory, is used for obtaining GNSS data. Seven BDS and GPS satellites are selected, specifically satellites C05, C02, C28, C41, G32, G04, and G16. The BDS B1I data at 2:00:00 on September 5, 2023 and the GPS L1 C/A data at 13:00:00 on September 5, 2023 are used for analysis. The values of $\theta_{El,A}$ for these satellites are shown in Table 1. The higher elevation is about 20° or 30° higher than the lower one, to ensure an approximate uniform distribution of elevation ranging from 15° to 90°.

Both position A and position B are described in the local Cartesian coordinate system (E, N, U). Position A of BJ02 is calculated by the PPP technique.

In experiment 1, time transfer experiments with the real BDS and GPS signal and the Monte Carlo simulation experiments are designed. ΔE, ΔN and ΔU, ranging from −5000 m to 5000 m, are added to position A to generate position B. The software R2CGGTTSv8.8 is used to generate the 30-second files in Common GNSS Generic Time Transfer Standard (CGGTTS) format. The REFSYS values in these files with position A and position B are differentiated to represent ΔT_{L-G}. ΔT_{tropo} and ΔT_{iono} are calculated based on MDTR and MDIO values in CGGTTS files,

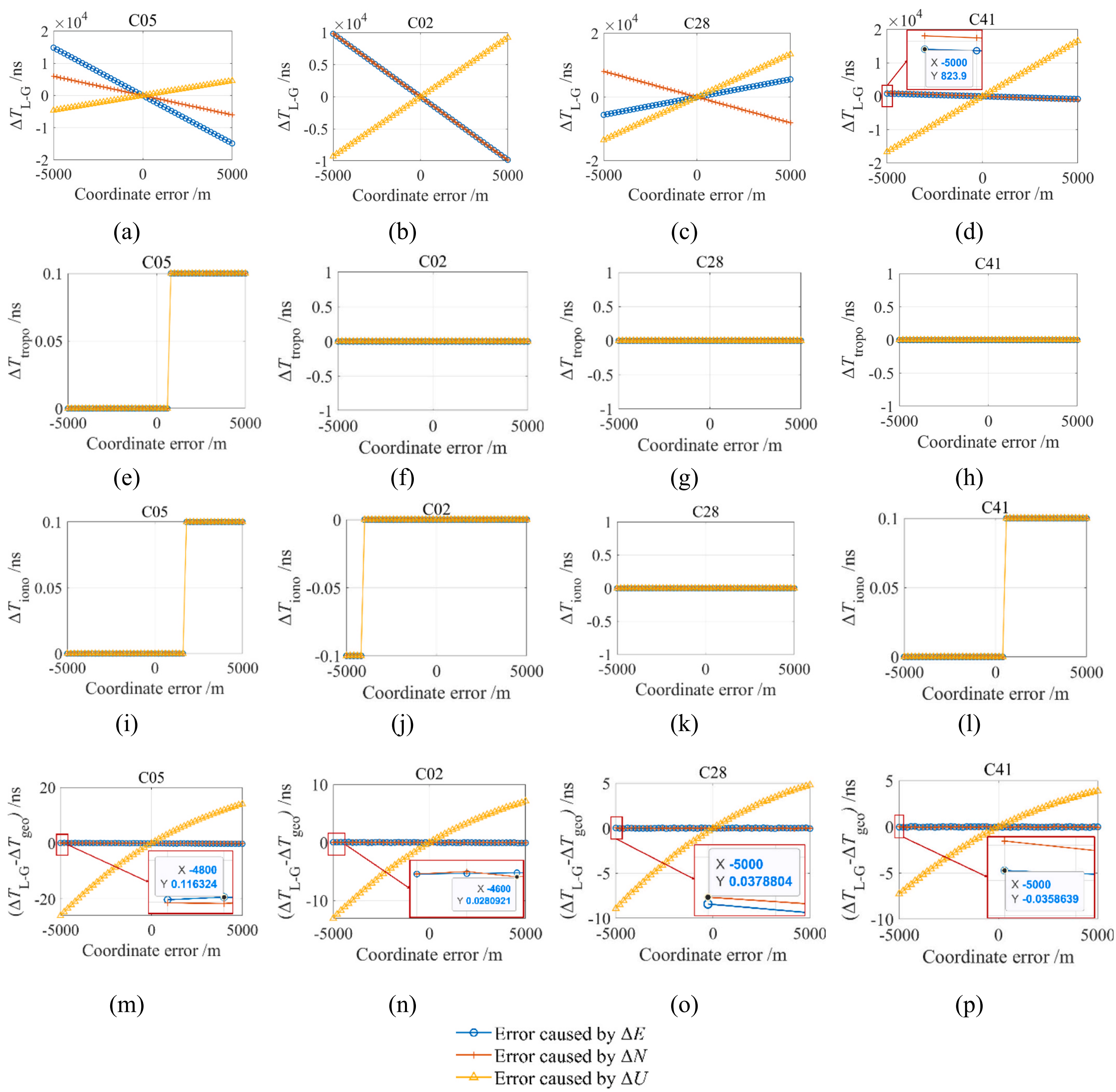

Fig. 19. (a)~(d) ΔT_{L-G} of the satellites C05, C02, C28 and C41. (e)~(h) ΔT_{tropo} of the satellites C05, C02, C28 and C41. (i)~(l) ΔT_{iono} of the satellites C05, C02, C28 and C41. (m)~(p) The differences between ΔT_{L-G} and ΔT_{geo} of the satellites C05, C02, C28 and C41.

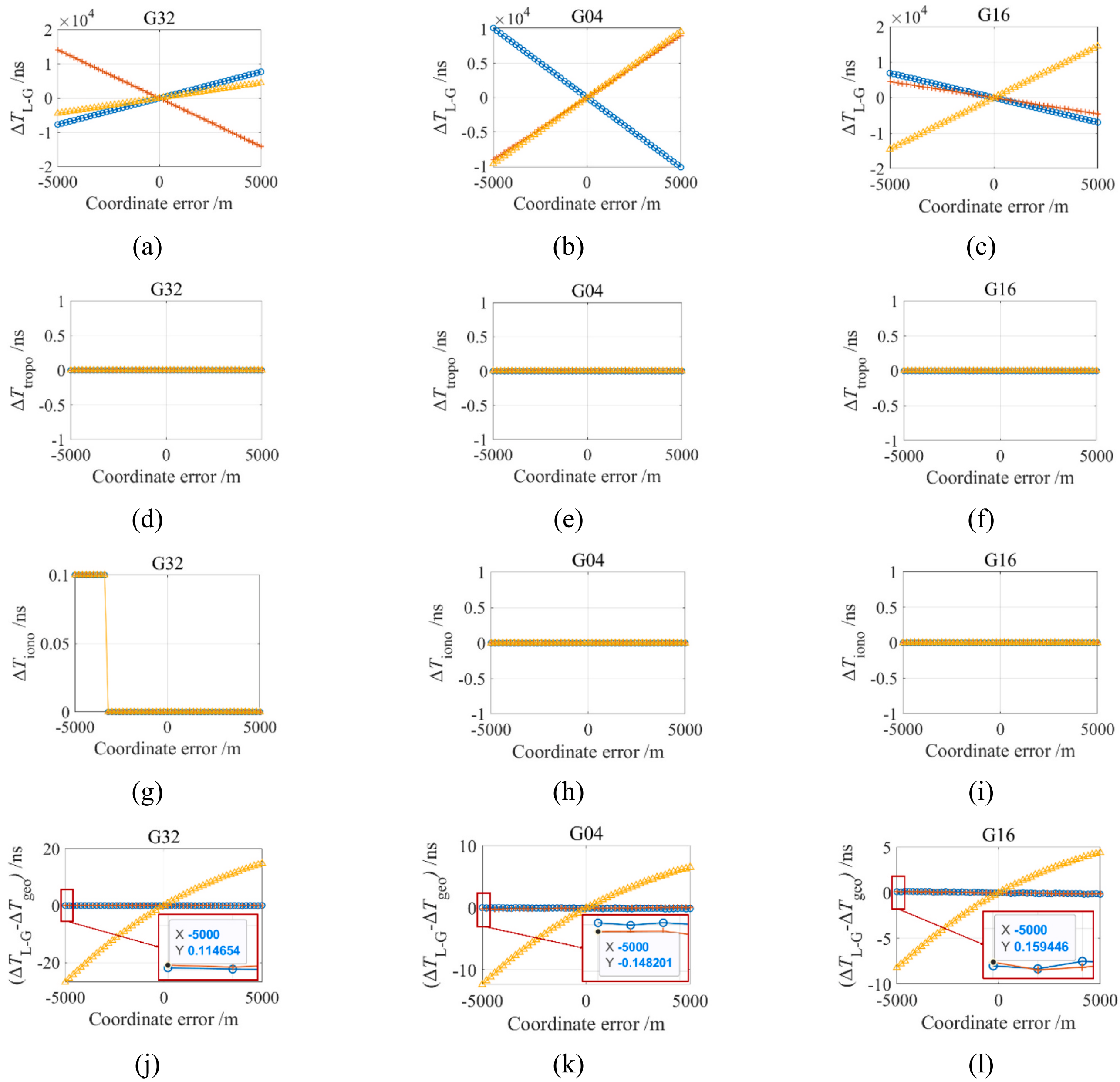

Fig. 20. (a)~(c) ΔT_{L-G} of the satellites G32, G04 and G16. (d)~(f) ΔT_{tropo} of the satellites G32, G04 and G16. (g)~(i) ΔT_{iono} of the satellites G32, G04 and G16. (j)~(l) The differences between ΔT_{L-G} and ΔT_{geo} of the satellites G32, G04 and G16.

respectively.

In experiment 2, the cases with the coordinate error of −5000 m/5000 m are selected. The true time transfer error is ΔT_{L-G} calculated in experiment 1, and the theoretical time transfer error is calculated by (16) or the fitted cosine function. The residual is represented by the absolute value of the difference between the theoretical and the true time transfer errors.

4.2. Results and discussion

4.2.1. Experiment 1

ΔT_{L-G},ΔT_{tropo}, ΔT_{iono} and ΔT_{geo} of the BDS and the GPS satellites caused by ΔE, ΔN and ΔU are shown in Fig. 19(a)–(l) and Fig. 20(a)–(i). The higher $\theta_{El,A}$ of the satellites is, the larger ΔT_{L-G} caused by ΔU, since θ_{EA} is close to 0° or 180°. On the contrary, the effects of ΔN and ΔE on ΔT_{L-G} reduce since θ_{EA} approaches 90°. From the absolute value of ΔT_{L-G} for the satellite C41, ΔT_{L-G} caused by ΔE is the smallest among all BDS and GPS cases, which is 823.9 ns when ΔE is −5000 m. The jump values of 0.1 ns in ΔT_{tropo} and ΔT_{iono} are due to the 0.1 ns resolution of MDTR values and MDIO values. The absolute values of ΔT_{tropo} and ΔT_{iono} within the coordinate error of 5000 m do not exceed 0.1 ns, which are much smaller than ΔT_{L-G} and can be negligible. The differences between ΔT_{L-G} and ΔT_{geo} of the BDS and the GPS satellites are shown in Fig. 19(m)–(p) and Fig. 20(j)–(l), which are much smaller than ΔT_{L-G}, indicating that the geometric distance delay error is the main cause of the time transfer error. Since ΔE, ΔN and ΔU are added to position A respectively, the coordinate error can be treated as the position error. The linear relationship between ΔT_{L-G} and the position error can be seen in each case, which is consistent with the theoretical analysis.

4.2.2. Experiment 2

θ_{EA} can be calculated based on the known coordinates of the satellites, position A, and position B. The true values of ΔT_{L-G} are derived from the results of experiment 1 shown in Fig. 19 and Fig. 20. Tables 2

Table 2
The theoretical and the true values of ΔT_{L-G} for C05, C02, C28, and C41.

PRN		Coordinate error /m					
		ΔE = -5000	ΔE = 5000	ΔN = -5000	ΔN = 5000	ΔU = -5000	ΔU = 5000
C05	$\theta_{EA}/°$	26.9	153.1	68.9	111.1	105.9	74.1
	Theoretical ΔT_{L-G} /ns	14871.5	−14872.4	6004.5	−6008.1	−4574.8	4571.0
	True ΔT_{L-G} /ns	14871.8	−14872.4	6005.4	−6007.3	−4599.9	4586.0
	Residual /ns	0.3	0	0.9	0.8	25.1	15.0
C02	$\theta_{EA}/°$	54.0	126.0	53.8	126.2	123.6	56.4
	Theoretical ΔT_{L-G} /ns	9807.6	−9810.5	9838.2	−9841.1	−9227.9	9224.9
	True ΔT_{L-G} /ns	9808.4	−9809.8	9839.0	−9840.4	−9240.2	9232.8
	Residual /ns	0.8	0.7	0.8	0.7	12.3	7.9
C28	$\theta_{EA}/°$	109.6	70.4	61.0	119.0	143.9	36.1
	Theoretical ΔT_{L-G} /ns	−5586.0	5579.4	8089.2	−8094.9	−13474.0	13471.4
	True ΔT_{L-G} /ns	−5584.3	5581.0	8090.7	−8093.5	−13482.3	13476.9
	Residual /ns	1.7	1.6	1.5	1.4	8.3	5.5
C41	$\theta_{EA}/°$	87.2	92.8	86.1	93.9	175.2	4.8
	Theoretical ΔT_{L-G} /ns	822.0	−829.7	1116.4	−1124.1	−16620.1	16620.0
	True ΔT_{L-G} /ns	823.9	−827.8	1118.3	−1122.2	−16627.3	16623.9
	Residual /ns	1.9	1.9	1.9	1.9	7.2	3.9

Table 3
The theoretical and the true values of ΔT_{L-G} for G32, G04 and G16.

PRN		Coordinate error /m					
		ΔE = -5000	ΔE = 5000	ΔN = -5000	ΔN = 5000	ΔU = -5000	ΔU = 5000
G32	$\theta_{EA}/°$	117.6	62.4	32.2	147.8	105.4	74.6
	Theoretical ΔT_{L-G} /ns	−7718.2	7712.8	14108.9	−14110.9	−4424.2	4417.7
	True ΔT_{L-G} /ns	−7716.8	7714.2	14109.5	−14110.4	−4449.5	4434.2
	Residual /ns	1.4	1.4	0.6	0.5	25.3	16.5
G04	$\theta_{EA}/°$	52.5	127.5	122.9	57.1	125.3	54.7
	Theoretical ΔT_{L-G} /ns	10156.2	−10160.9	−9050.0	9044.7	−9652.0	9647.0
	True ΔT_{L-G} /ns	10157.4	−10159.8	−9048.8	9046.1	−9663.1	9654.8
	Residual /ns	1.2	1.1	1.2	1.4	11.1	7.8
G16	$\theta_{EA}/°$	65.4	114.6	74.2	105.8	150.2	29.8
	Theoretical ΔT_{L-G} /ns	6931.7	−6938.4	4533.0	−4540.5	−14474.6	14472.6
	True ΔT_{L-G} /ns	6933.5	−6936.9	4535.0	−4538.7	−14482.3	14477.5
	Residual /ns	1.8	1.5	2.0	1.8	7.7	4.9

and 3 show the theoretical ΔT_{L-G} calculated by (16) and the true ΔT_{L-G} at the coordinate error of −5000 m/5000 m of the BDS and the GPS satellites. The maximum residual is about 183 times smaller than the absolute value of the true ΔT_{L-G}, which shows that the theoretical ΔT_{L-G} and the true ΔT_{L-G} are well consistent, indicating that the time transfer error caused by the position error can be estimated by (16) effectively. Tables 4 and 5 show the amplitude values of the fitted cosine functions and the residuals. The fitted cosine function, which takes the form of (17), is calculated based on θ_{EA} and the true ΔT_{L-G} of each satellite by ordinary least squares. The maximum residual 29.1 ns is about 158 times smaller than the absolute value of the true ΔT_{L-G} 4599.9 ns. It is demonstrated that the cosine function can be utilized to describe the relationship between θ_{EA} and ΔT_{L-G}.

5. Conclusion

The error sources related to the position of the time transfer station in GNSS time transfer are analyzed individually to describe how they affect time transfer and quantify the impact of the position on GNSS time transfer. The coordinate vectors of the receiver and the satellite are defined. The method for mapping them to GNSS time transfer is proposed. The error angle, defined based on the receiver and the satellite coordinate vector, is used to quantify the impact. The correction terms for the errors related to the receiver coordinates include the geometric distance delay, the ionospheric delay, and the tropospheric delay. The geometric distance delay error, which is two and four orders of magnitude larger than the tropospheric delay error and the ionospheric delay error separately, is the main cause of the time transfer error. An analytical expression describing the relationship between them is derived. For the identical value of the position error, the time transfer error induced by the position error is different for different directions with respect to the true position. The time transfer error is maximized at 3.3 ns per meter of the position error when the error angle is 0° or 180°, and minimized when the error angle is 90°. However, maximum time transfer error is constrained to 3.3 ns with the position error of one meter. When the error angle is constant, there is an approximately linear relationship between the time transfer error and the position error. When the position error is constant, the time transfer error follows approximately a cosine relationship with the error angle.

CRediT authorship contribution statement

Baoying Wei: Writing – original draft, Visualization, Validation, Software, Resources, Project administration, Methodology, Investigation, Formal analysis, Data curation, Conceptualization. **Kun Liang:** Validation, Supervision, Resources, Project administration,

Table 4
The amplitude values and residuals for C05, C02, C28, and C41.

PRN		Coordinate error /m					
		$\Delta E=$ -5000	$\Delta E=$ 5000	$\Delta N=$ -5000	$\Delta N=$ 5000	$\Delta U=$ -5000	$\Delta U=$ 5000
C05	Amplitude /ns	16684.2					
	Residual /ns	7.1	6.5	0.9	1.0	29.1	15.2
C02	Amplitude /ns	16679.3					
	Residual /ns	4.6	6.0	11.9	10.5	10.0	2.6
C28	Amplitude /ns	16680.3					
	Residual /ns	11.1	14.4	3.9	6.7	4.8	0.6
C41	Amplitude /ns	16683.7					
	Residual /ns	8.9	12.8	16.4	12.5	2.2	1.2

Table 5
The amplitude values and residuals for G32, G04 and G16.

PRN		Coordinate error /m					
		$\Delta E=$ -5000	$\Delta E=$ 5000	$\Delta N=$ -5000	$\Delta N=$ 5000	$\Delta U=$ -5000	$\Delta U=$ 5000
G32	Amplitude /ns	16673.8					
	Residual /ns	8.1	10.7	0.3	1.2	21.7	6.4
G04	Amplitude /ns	16687.5					
	Residual /ns	1.3	1.1	15.4	18.1	20.1	11.8
G16	Amplitude /ns	16680.1					
	Residual /ns	10.1	6.7	6.6	2.9	7.9	3.1

Methodology, Funding acquisition, Conceptualization. **Jian Wang:** Supervision. **Zhiyu He:** Supervision, Resources. **Yufeng Li:** Formal analysis, Conceptualization. **Junliang Zhao:** Supervision, Software, Resources, Methodology, Formal analysis.

Declaration of competing interest

The authors declare that they have no known competing financial interests or personal relationships that could have appeared to influence the work reported in this paper.

Acknowledgements

This work was supported by the National Natural Science Foundation of China with Grant No. 12473072, the TaiShan Industrial Experts Programme (tscx202408155), the Yantai Major Science&Technology Innovation and Development Project (2024ZDCX002) and the Open Foundation of The Center of National Railway Intelligent Transportation System Engineering and Technology (2023YJ360).

Data availability

Data will be made available on request.

References

[1] White Paper: Application Technology of Next Generation Railway Carrying Network, China Railway Society, 2020.
[2] P. Defraigne, G. Petit, Time transfer to TAI using geodetic receivers, Metrologia 91 (4) (2003).
[3] G. Petit and Z. Jiang, "Stability and accuracy of GPS P3 TAI time links," *2004 18th European Frequency and Time Forum (EFTF 2004)*, Guildford, 2004, pp. 287-291, doi: 10.1049/cp:20040870.
[4] P. Defraigne and K. Verhasselt, "Multi-GNSS time transfer with CGGTTS-V2E," *2018 European Frequency and Time Forum (EFTF)*, Turin, Italy, 2018, pp. 270-275, doi: 10.1109/EFTF.2018.8409047.
[5] G. Xu and Y. Xu,"GPS: Theory, algorithms and applications" 3rd ed, 2016.
[6] J. Saastamoinen, Atmospheric correction for the troposphere and stratosphere in radio ranging satellites, Use Artif. Satellites Geodesy 15 (1972).
[7] H.S. Hopfield, Tropospheric range error parameters: further studies, No. APL/JHU-CP-015 (1972).
[8] A.E. Niell, 1996 Global mapping functions for the atmosphere delay at radio wavelengths, J. Geophys. Res.: Solid Earth 101 (1996).
[9] J. Böhm, A.E. Niell, P. Tregoning, H. Schuh, Global Mapping Function (GMF): A new empirical mapping function based on numerical weather model data, *Geophys. Res. Lett.* 33 (2006).
[10] J. Böhm, B. Werl, H. Schuh, Troposphere mapping functions for GPS and very long baseline interferometry from European Centre for Medium-Range Weather Forecasts operational analysis data, J. Geophys. Res.: Solid Earth 111 (2006).
[11] Q. Baire, P. Defraigne and E. Pottiaux, "Influence of troposphere in PPP time transfer," *2009 IEEE International Frequency Control Symposium Joint with the 22nd European Frequency and Time forum*, Besancon, France, 2009, pp. 1065-1068.
[12] N. Wang, Y. Yuan, Z. Li, X. Huo, Improvement of Klobuchar model for GNSS single-frequency ionospheric delay corrections, *Adv. Space Res.* 57 (2016).
[13] K.C.T. Swamy, A.D. Sarma, A. Supraja Reddy, V. Satya Srinivas, P.V.D. Somasekhar Rao, Modelling of GPS signal scintillations with polynomial coefficients over the Indian region, Indian J. Radio Space Phys. (IJRSP) IJRSP 42 (3) (2013).
[14] K.C.T. Swamy, V.R. Devanaboyina, R. Nallagarla, T.A. Shaik, S. Turpati, Correlation between rate of TEC index and positioning error during solar flares and geomagnetic storms using navigation with Indian constellation receiver measurements, J. Appl. Geodesy (2024).
[15] S. Pireaux, P. Defraigne, L. Wauters, N. Bergeot, Q. "Baire and C. Bruyninx, Higher-order ionospheric effects in GPS time and frequency transfer". *GPS Solutions*, 14, 267–277.
[16] K.C.T. Swamy, D. Venkata Ratnam, T. Suman, T.A. Shaik, Time-differenced double difference method for measurement of Navigation with Indian Constellation (NavIC) receiver differential phase bias, *Measurement* 207 (2023) 112385.
[17] G. Petit, J. Zhiheng, P. Uhrich, F. Taris, "Differential calibration of Ashtech Z12-T receivers for accurate time comparisons", *The 14th European Frequency and Time Forum (EFTF)*, Turin, Italy, May, 2000.
[18] A. Proia, G. Cibiel, J. White, D. Wilson, K. Senior, "Absolute calibration of GNSS time transfer systems: NRL and CNES techniques comparison". *2011 Joint Conference of the IEEE International Frequency Control and the European Frequency and Time Forum (IFCS) Proceedings*, 2011, pp. 1-6.
[19] J. Delporte, D. Valat, "CNES Accurate monitoring of GNSS time scales based on absolute calibration". *2022 Joint Conference of the European Frequency and Time Forum and IEEE International Frequency Control Symposium*, Paris, France, 24-28 Apr. 2022, pp. 1–5.
[20] D. Valat, J. Delporte, Absolute calibration of timing receiver chains at the nanosecond uncertainty level for GNSS time scales monitoring, *Metrologia* 57 (2020).
[21] E. Garbin, P. Defraigne, P. Krystek, R. Piriz, B. Bertrand, P. Waller, Absolute calibration of GNSS timing stations and its applicability to real signals, *Metrologia* 56 (2019).
[22] I. Blinov, V. Fedoto, N. Koshelyaevsky. The First Absolute Delay Determination of GLONASS Time Receiver for TAI Time Transfer Link Calibration, *Proceedings of the 47th Annual Precise Time and Time Interval Systems and Applications Meeting.* Monterey, California, 25-28 Jan. 2016, pp. 223-230.
[23] H. Chadsey, How Bad Receiver Coordinates Can Affect GPS Timing, in: Proceedings of the 27th Annual Precise Time and Time Interval Systems and Applications Meeting, United States of America, San Diego, California, 1995, pp. 135–144.
[24] Z. Ren, X. Huang, H. Gong, J. Peng, G. Sun, BDS-3 RDSS two-way time transfer with asymmetric delay compensation model, *Meas. Sci. Technol.* 34 (2022).
[25] P. Defraigne, G. Petit, CGGTTS-Version 2E: an extended standard for GNSS time transfer, *Metrologia* 52 (2015).
[26] BeiDou Navigation Satellite System Open Service Performance Standard (Version 3.0), BDS-OS-PS-3.0, China Satellite Navigation Office, 2016.